

Fermi-liquid effects in the gapless state of marginally thin superconducting films

G. Catelani

Department of Physics and Astronomy, Rutgers University, Piscataway, New Jersey 08854, USA

X. S. Wu* and P. W. Adams

Department of Physics and Astronomy, Louisiana State University, Baton Rouge, Louisiana 70803, USA

(Dated: October 31, 2018)

We present low temperature tunneling density-of-states measurements in Al films in high parallel magnetic fields. The thickness range of the films, $t = 6 - 9$ nm, was chosen so that the orbital and Zeeman contributions to their parallel critical fields were comparable. In this quasi-spin paramagnetically limited configuration, the field produces a significant suppression of the gap, and at high fields the gapless state is reached. By comparing measured and calculated tunneling spectra we are able to extract the value of the antisymmetric Fermi-liquid parameter G^0 and thereby deduce the quasiparticle density dependence of the effective parameter G_{eff}^0 across the gapless state.

PACS numbers: 74.78.Db, 73.40.Jn, 74.25.-q

I. INTRODUCTION

One of the most successful constructs in condensed matter physics is Landau's Fermi-liquid (FL) description of the low temperature properties of interacting electron systems.^{1,2} The theory provides for the salient thermodynamic and transport properties of a profoundly complex many-body system in terms of a low-density gas of quasiparticle excitations. The averaged effects of electron-electron and electron-phonon interactions are incorporated into a number of FL parameters, which are associated with the renormalization of fundamental system properties such as the effective mass and the spin susceptibility.³ In particular, the so-called antisymmetric FL parameter G^0 affects the spin response of the system and is related to the ratio of the spin susceptibility density of states $N(\chi)$ to the heat-capacity density of states $N(\gamma)$ by $G^0 = N(\gamma)/N(\chi) - 1$.³ In this paper we report low-temperature measurements of the parameter G^0 in superconducting disordered Al films.

Although G^0 is a fundamentally important parameter in the many-body description of metals, there have been very few measurements of it reported in the literature. This is due, in part, to the fact that it is difficult to measure it directly in bulk systems. Consequently, little is known about its dependence on disorder, quasiparticle density, and/or dimensionality. Measurements of G^0 have been extracted from high-field tunneling density of states (TDOS) and critical-field studies of low atomic mass superconducting films. For example, estimates of normal-state value of G^0 have been reported via tunneling studies of the Zeeman splitting of the BCS density of states in superconducting Al films, $G^0 \sim 0.3 - 0.4$,^{4,5} in the intermediate to high-temperature regime where the superconducting order parameter is partly suppressed by thermal fluctuations. Low-temperature TDOS measurements in amorphous Ga films, which are strong-coupling superconductors, give a somewhat larger value of $G^0 \sim 0.81$.⁶ Alternatively, G^0 can be extracted from parallel critical field measurements. This method gives

$G^0 \sim 0.23$ in TiN films.⁷ The only direct measurements of G^0 have been obtained in the normal state, via the field dependence of the pairing resonance⁸ in Al, $G^0 \sim 0.17$,⁹ and Be films, $G^0 \sim 0.21$.¹⁰ In all these systems the spin-orbit scattering is quite low; thus, spin remains a good quantum number.

In the experiments described above the films were sufficiently thin so as to suppress the Meissner currents; therefore the field response was purely due to the electron Zeeman splitting (see e.g. Ref. 11 and Sec. II). By contrast, in this work we consider thicker films; this enables us to explore the gapless state and determine G^0 from low temperature TDOS measurements. In the normal state, the internal field H_i felt by the electron spins is given by $H_i = H + H_{\text{ex}}$, where H is the applied field and the exchange field is $H_{\text{ex}} = -HG^0/(1+G^0)$. Deep in the superconducting phase, *i.e.*, at low temperature and low field, the number of quasiparticles is small due to the fact that they have been consumed by the formation of the superconducting condensate. In this limit, the exchange effects are greatly suppressed and the effective Landau parameter [see Eq. (6)] is small compared to its normal state value, $G_{\text{eff}}^0 \sim 0$. However, as one approaches the critical field $H_{c||}$, the quasiparticle density increases and $G_{\text{eff}}^0 \rightarrow G^0$. Below we show that the main features of the TDOS in the gapless superconducting state are strongly influenced by the rise of these exchange interactions. In addition to its fundamental interest, a thorough understanding of exchange effects in superconducting Al films is important for possible applications in mesoscopic hybrid structures aimed at the control of current spin polarization via the Zeeman splitting in the superconducting elements.¹²

This paper is organized as follows: in Sec. II we give a brief overview of the phase transition in thin films and introduce the parameters necessary for the description of its properties. In Sec. III we give some details of the samples' preparation, and in Sec. IV we discuss our main results.

II. PHASE TRANSITION IN MARGINALLY THIN FILMS

In bulk superconductors the critical-field transition is completely dominated by the orbital response of the conduction electrons.¹³ It is possible, however, to inhibit the orbital response by applying a magnetic field in the plane of a superconducting film whose thickness t is much less than the superconducting coherence length ξ and whose electron diffusivity is low.^{11,14,15} Under these conditions the phase transition to the normal state is mediated by the spin polarization of the electrons, and at the critical field the electron Zeeman splitting is of the order of the superconducting gap energy. At zero temperature, in particular, a first-order transition from the superconducting state to the paramagnetic normal state occurs at the Clogston-Chandrasekhar critical field^{16,17}

$$H_{c||}^{CC} = \frac{\Delta_o \sqrt{1 + G^0}}{\sqrt{2} \mu_B}, \quad (1)$$

where Δ_o is the zero-field, zero-temperature gap energy, and μ_B is the Bohr magneton. This so-called ‘‘spin-paramagnetic’’ (S-P) transition is realized in low atomic mass superconductors such as Al, Be, and TiN, and it is accompanied by very peculiar dynamics.^{9,11,18,19,20} Note that for positive G^0 the parallel critical field exceeds the non-interacting Clogston-Chandrasekhar limit.

In the thin-film limit and at low temperatures, the parallel magnetic field has little effect on the order parameter up to the transition, and the Clogston-Chandrasekhar critical field [Eq. (1)] can be more than an order of magnitude higher than its orbitally-mediated counterpart. However, if the thin film condition is marginally relaxed then orbital effects will generally lower the critical field. A measure of the relative weight of the orbital response compared to the spin polarization in determining the parallel critical field is given by the dimensionless orbital pair-breaking parameter¹¹

$$c = \frac{D(et)^2 \Delta_o}{6\hbar\mu_B^2} f(\ell/t), \quad (2)$$

where D is the electron diffusivity, t is the film thickness, e is the electron charge, and ℓ is the mean-free path for impurity scattering. The function $f(\ell/t)$ describes the crossover between local electrodynamic response of the film for $\ell \ll t$, where $f(\ell/t) \rightarrow 1$, and the non-local one in the opposite limit $\ell \gg t$, where $f(\ell/t) \simeq 3t/4\ell$.²¹ For marginally thin films used in this study, $c \sim 1$.

Beside the film’s thickness (through the parameter c) and exchange effects, spin-orbit scattering also affects the value of the parallel critical field. Therefore, following Ref. 11, we introduce a third dimensionless parameter $b = \hbar/3\Delta_o\tau_{so}$, where $1/\tau_{so}$ is the spin-orbit scattering rate. As remarked in Sec. I, in the materials under consideration spin-orbit scattering is a small effect, $b \ll 1$. The three parameters c , G^0 , and b ,

can have competing effects on the value of the parallel critical field. Moreover, they also affect the position of the tricritical point separating the low-temperature first-order phase transition from the higher-temperature second-order one. In the limit $G^0, c \rightarrow 0$ the tricritical temperature is $T_{tri} \simeq 0.56T_c$, where T_c is the critical temperature.¹¹ More generally, the tricritical temperature and other properties of a superconducting film, such as the TDOS, can be calculated by solving the Usadel equations for the semiclassical Green’s functions together with the self-consistent equations for the order parameter δ and the internal magnetic field H_i ; these equations can be found in Ref. 4 (see also Ref. 7 for an alternative parametrization). All three dimensionless parameters enter into these mean field equations, while Δ_o (or $T_c \simeq 0.57\Delta_o/k_B$) fixes the overall energy scale.

In this work we present low temperature measurements of TDOS in Al films whose thicknesses are about two to three times greater than the $t \sim 3$ nm typically used in spin-paramagnetic studies.²² Though the thickness of the films remains much smaller than the superconducting coherence length, $t \ll \xi$, the orbital response to the applied field is no longer negligible. Indeed, the thickness range is chosen to assure that the orbital and Zeeman contributions to the critical field are comparable (this could also be accomplished by rotating the films out of parallel orientation, but a finite perpendicular field component would introduce vorticity²³). Interestingly, the critical field transition can become reentrant²⁴ under these conditions. The reentrance is associated with a high-entropy gapless state near the critical field, in which the superconducting state has higher entropy than the normal state.²⁵ The primary purpose of the present work is to determine G^0 through TDOS measurements across the gapless region, where there is a monotonic increase in quasiparticle density as one approaches the second-order phase transition to the normal state.

III. SAMPLE PREPARATION

Aluminum films were fabricated by e-beam deposition of 99.999% Al onto fire polished glass microscope slides held at 84 K. The depositions were made in a typical vacuum $P < 3 \times 10^{-7}$ Torr at a rate of ~ 0.2 nm/s. Films with thicknesses ranging from 6 to 9 nm had normal-state sheet resistances that ranged from $R = 10$ to 20Ω at 100 mK. After deposition, the films were exposed to the atmosphere for 0.5-4 h in order to allow a thin native oxide layer to form. On top of the oxide, serving as the tunneling barrier, a 14-nm-thick Al counterelectrode was deposited. Due to its relatively large thickness, the counterelectrode had a parallel critical field of ~ 1.1 T, which is to be compared with $H_{c||} \sim 3$ T for the films. The junction resistance ranged from 10 to 20 k Ω , depending on exposure time and other factors, for a junction area of about 1×1 mm². Only junctions with resistances much greater than that of the films were used. Magnetic

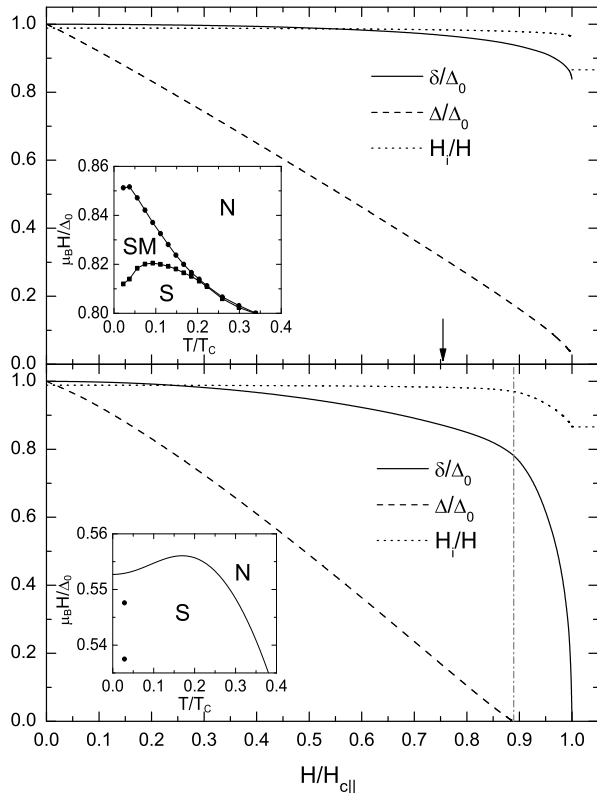


FIG. 1: Upper panel: Calculated field dependencies of the superconducting order parameter δ , gap Δ , and ratio between internal and applied fields H_i/H for a 2.5-nm-thick Al film ($T_c = 2.7$ K) in parallel field at 77 mK. The arrow indicates the theoretical supercooling field. Note that the gap is finite up to the superheating field. The upper inset is the corresponding phase diagram where S is the superconducting phase, N the normal state, and SM is the state memory region. Lower panel: Field dependencies of the same quantities for a 7-nm-thick Al film ($T_c = 2.1$ K) at 60 mK. The vertical dot-dashed line separates the gapped and gapless regions. Note in the latter the fast drop of the order parameter with increasing field. The lower inset is the corresponding phase diagram, with a maximum in the second-order critical-field curve. The two points in the phase diagram represent the temperature and fields at which tunneling spectra were taken in the gapless region.

fields of up to 9 T were applied using a superconducting solenoid. An *in situ* mechanical rotator was employed to align the film surface parallel to the field with a precision of $\sim 0.1^\circ$. Measurements of resistance and tunneling were carried out in an Oxford dilution refrigerator using a standard ac four-probe technique.

IV. RESULTS AND DISCUSSION

Shown in the upper panel in Fig. 1 are the calculated low-temperature field dependencies of the order param-

eter δ , gap energy Δ , and internal field H_i for a 2.5-nm-thick Al film having $T_c = 2.7$ K, $\Delta_o/e = 0.41$ mV, $\xi \sim 15$ nm, and sheet resistance $R \sim 1$ k Ω . At this thickness and resistivity orbital effects are negligible, since we estimate $c \simeq 0.02 \ll 1$. Accordingly, δ and H_i/H are relatively insensitive to the applied field up to the first-order parallel critical field located approximately half way between the supercooling field (arrow in figure) and the superheating one (used for normalization in the upper panel). In contrast the gap Δ , while remaining finite, decreases linearly as expected because even a small spin-orbit scattering mixes the densities of states of opposite spins, which in turn are shifted in opposite directions by the Zeeman field. The curves are computed by numerically solving the mean-field equations mentioned in Sec. II; for concreteness, we use for the spin-orbit scattering parameter $b = 0.052$, and for the Fermi-liquid parameter $G^0 = 0.155$, as these values are the one we extract from the measurements in thicker films. Shown in the inset of the upper panel of Fig. 1 is the measured parallel critical field of this film as a function of temperature. This plot represents the classic S-P phase diagram in which a high-temperature line of second-order phase transitions crosses over into a line of first-order transitions at the tricritical point $T_{tri} \sim 0.3T_c$.¹⁵

In the lower panel of Fig. 1 we show the corresponding behavior of δ , Δ , and H_i at 60 mK for a 7-nm-thick Al film having $T_c \simeq 2.1$ K, $\Delta_o/e \simeq 0.32$ mV, $\xi \simeq 60$ nm,²⁶ and $R = 16 \Omega$. Not only does this thicker film have a lower critical field due to its finite orbital response, but also the structure of its phase diagram (lower inset) is dramatically altered from that of the classic S-P diagram. Indeed, due to the local maximum in the parallel critical field near $T/T_c = 0.45$, the critical-field behavior is reversibly reentrant.²⁵ The most obvious difference between the field dependencies shown in the upper and lower panels of Fig. 1 is that the gap energy in the thicker film goes to zero before the critical field is reached. In fact, the region to the right of the vertical dot-dashed line represents a gapless superconducting state; clearly, in this region rapid changes in δ and H_i take place.

Deep in the superconducting phase, where the superconducting order parameter is well established, exchange effects are negligible due to the fact that the quasiparticle density is low and the e - e interaction effects parametrized by G^0 are preempted by the formation of the condensate. Interestingly, however, it is clear in both panels of Fig. 1 that H_i/H never reaches unity in the limit of small applied field. We believe that this is a spin-orbit effect, and that, in the zero-temperature zero-field limit $H_i/H = 1/[1 + G^0\alpha(b)]$, where $\alpha(b)$ is a positive function of the spin-orbit parameter b . $\alpha(b)$ goes linearly to zero as $b \rightarrow 0$ and saturates to 1 in the limit $b \rightarrow \infty$. Once the field is increased beyond the onset of the gapless state, the quasiparticle density rapidly grows until it reaches its normal-state value at $H_{c||}$ as we discuss in more detail below. Similarly, exchange effects, as reflected in the internal field, also begin to “turn on” upon

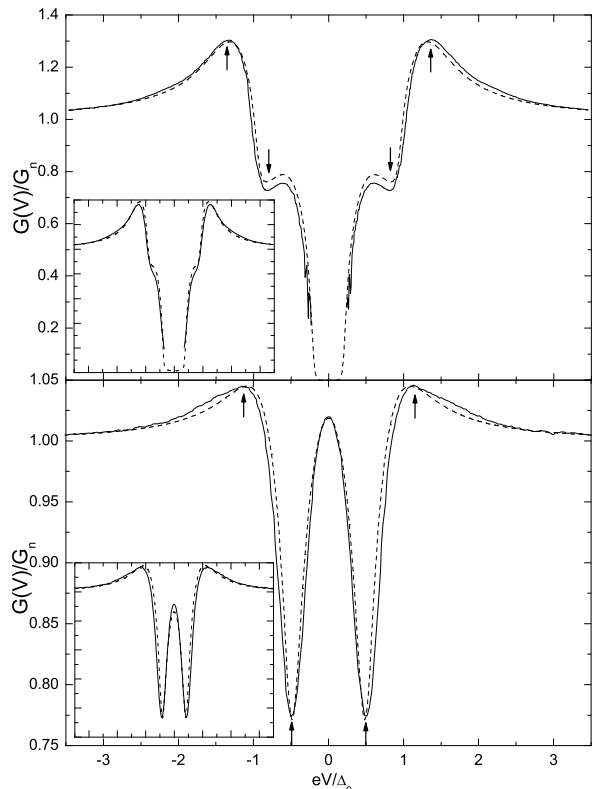


FIG. 2: Tunneling conductance normalized by the normal-state conductance G_n as a function of normalized bias voltage. The solid lines are experimental spectra of a 7-nm-thick Al film taken at 60 mK in a parallel field of 2.20 (upper panel, gapped) and a 3.02 T (lower panel, gapless). The dashed curves are the calculated spectra – see the text for more details. The arrows point to the primary peak and dip features of the spectra. The insets show spectra for an 8-nm-thick film taken at 1.40 (upper inset) and 2.42 T (lower one); the axes cover the same ranges as the respective main panels. The dashed lines are the theoretical curves hardly distinguishable from the continuous experimental lines.

entering the gapless state. In contrast, in the purely S-P limit, there is no gapless state, and the internal field jumps discontinuously to its normal-state value at the first-order critical-field transition (see the upper panel of Fig. 1).

In Fig. 2 we compare the normalized tunneling conductances obtained in the gapped and gapless states of the 7 nm Al film at 60 mK. The upper panel was taken at $H = 2.2$ T corresponding to the gapped phase. The curve clearly displays a Zeeman splitting of the BCS density-of-states peaks.¹⁴ The data in the lower panel of Fig. 2 were measured at 3.02 T. Note that the gap is completely suppressed and that a large number of states exist at the Fermi energy (*i.e.*, $V=0$). The dashed lines in Fig. 2 are the theoretical curves calculated with parameters $c = 0.79$, $G^0 = 0.155$, and $b = 0.052$.²⁵ We also

find good agreement between theory and experiment for TDOS measurements (see insets of Fig. 2) in an 8-nm-thick film with $c \simeq 1.23$; this value is in reasonable agreement with the scaling $c \propto t^3$ of Eq. (2) in the non-local limit relevant to these samples.²⁵ In the lower panel, an additional broadening,²⁷ $\Gamma = 0.016\Delta_o \simeq 5 \times 10^{-6}$ eV, is used in calculating the theoretical curve; *i.e.*, the relation between density of states ν and Green's function \mathcal{G} is taken to be $\nu(\epsilon) \propto \text{Im} \mathcal{G}(\epsilon + i\Gamma)$. A broadening of similar magnitude ($\Gamma = 0.01\Delta_o$) is used for the calculated curves in both insets. This finite broadening is larger than values reported in the literature,²⁸ but at these fields it could be caused by a small misalignment of the sample. Indeed, the Cooper pair cyclotron frequency associated with a field misalignment of angle θ with respect to the sample plane is $\hbar\Omega_{c\perp} = 4eDH \sin \theta$; at $\theta = 0.1^\circ$ and $H = 3$ T, and using the estimate $D \simeq 25$ cm²/s, we obtain $\hbar\Omega_{c\perp} \simeq 5 \times 10^{-5}$ eV $> \Gamma$. We also note that small variations in the parameters c and Γ can compensate each other. On one hand this seems to support the idea that in the present case Γ could be caused by an orbital effect of the field as c is; on the other hand this interdependence makes it difficult to extract Γ from the data²⁹ and a more thorough study of the broadening, including low-field measurements and/or intentional tilting, is necessary to verify this interpretation.

Although the two tunneling spectra in Fig. 2 are very different in structure, the evolution of the spectra as one moves from the gapped to the gapless state is continuous. The salient peak and dip features of each spectra are denoted by the arrows in Fig. 2 (we point out that the small broadening Γ , introduced above, affects the amplitude but not the position of these features in the theoretical curves). The behavior of these features as one crosses over into the gapless state is shown in Fig. 3. The main panel depicts the low-temperature field dependence of the outermost coherence peaks along with data points corresponding to tunneling measurements. Interestingly, the position of the peaks is not monotonic in field, and the peaks move to lower energy in the gapless state. The dotted line is simply the Zeeman splitting, which represents the expected peak position if there were no orbital depairing and no exchange effects. We have verified numerically that, in contrast to the results for the marginally thin films, the peaks follow the bare Zeeman splitting with good approximation for the thinner film with $c = 0.02$, in agreement with low-temperature measurements in thinner films.¹⁴ The dashed curve is the expected peak position with orbital depairing but no exchange. This curve misses the data points badly while agreeing with the solid curve at low field indicating that G^0 plays a significant role in determining the tunneling density of states in the gapless state. Moreover, with $G^0 = 0$ the low-temperature phase transition is predicted to be first-order, in contrast to the experimental finding of a second-order transition. The inset of Fig. 3 shows the corresponding field dependence of the spectra dips. As is the case with the peaks, the evolution of the

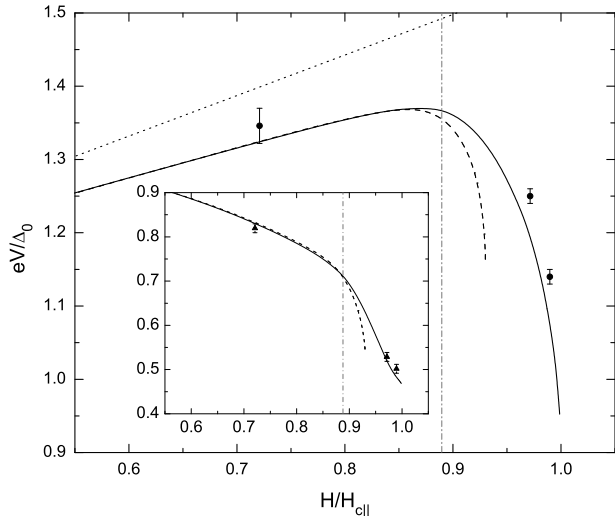


FIG. 3: Position of the peaks in Fig. 2 as a function of parallel field. The solid line represents the theoretical peak positions with Fermi-liquid effects included. Note that in the gapless state (right of the dot-dashed vertical line), the peaks move to lower energy as the field increases; this behavior is in agreement with the experimental measurements (circles with error bars). The dashed curve shows the theoretical peak positions in the case of no exchange, *i.e.*, $G^0 = 0$. The dotted line represents the Zeeman energy, which is the expected peak position with no exchange and no orbital pair breaking. Inset: Dip positions as a function of field. The solid line is the theoretical position including exchange, and the dashed line with exchange excluded. Triangles are data points.

dips' position contrasts with that of the thin-film case. In the latter, the dips follow the peaks to higher energies. In Fig. 3, the dips move to *lower* energy and the peaks broaden with increasing field. This broadening could potentially limit the degree of spin polarization that could be achieved in hybrid structures.¹²

Building on the above analysis we can now extract an “effective” FL exchange parameter G_{eff}^0 as a function of the quasiparticle density n_n . In Fig. 4 we plot such a function, where we assume a two-fluid model in order to estimate n_n . In this phenomenological approach, the superconducting carrier density n_s is related to the penetration depth λ by

$$n_s \propto \lambda^{-2} \quad (3)$$

and the normal electron density is $n_n = 1 - n_s$. In disordered thin superconducting films the parallel field penetration depth is proportional (up to a weakly temperature dependent coefficient) to the penetration depth λ_L of a clean superconductor in the local limit [see, e.g., Eq. (3.136) of Ref. 13]. The latter depends on temperature approximately as

$$\lambda_L(\gamma) \propto \frac{1}{\sqrt{1-\gamma^2}}, \quad (4)$$

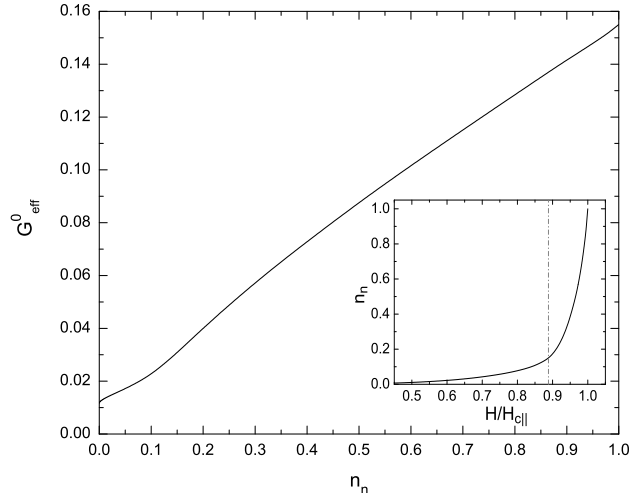


FIG. 4: Effective FL parameter G_{eff}^0 [Eq. (6)] as a function of quasiparticle density n_n in the superconducting phase of a marginally thin Al film. The inset is the calculated quasiparticle density as a function of the normalized parallel magnetic field for a 7-nm-thick Al film at 60 mK. The vertical dot-dashed line divides the gapped and gapless states. Note that in the latter region, the quasiparticle density quickly rises with the applied field.

where $\gamma = T/T_c$. Near the critical temperature, the temperature dependence of the order parameter is $\delta(\gamma)/\Delta_0 \propto \sqrt{1-\gamma}$. Inverting this relationship to express γ in terms of δ , substituting the result into Eq. (4), and using the definition of n_n , we arrive at:

$$n_n \propto \left(1 - \frac{\delta^2}{\Delta_0^2}\right)^2. \quad (5)$$

From this relation we evaluate the field dependence of the normal electron density through the calculated field dependence of the order parameter (at low temperature the proportionality constant can be taken to be unity up to exponentially small corrections); the result is presented in the inset of Fig. 4. We define the effective Fermi-liquid constant by

$$G_{\text{eff}}^0 = H/H_i - 1. \quad (6)$$

We can obtain this quantity from the calculated ratio H_i/H shown in Fig. 1. Note that G_{eff}^0 is approximately linear in the quasiparticle density, thus showing the gradual rise of exchange effects going from the superconducting to the normal phase. This microscopic calculation fully supports the qualitative explanation given in Ref. 9 for different g-factors in the superconducting and normal states, which correspond to $G_{\text{eff}}^0 = 0$ and $G_{\text{eff}}^0 \simeq 0.17$, respectively.

In summary, we have presented measurements of the tunneling density of states of marginally thin Al films in parallel magnetic field. The marginality condition $c \sim 1$, with the dimensionless parameter c defined in

Eq. (2), gives access to a gapless superconducting state. The inclusion of Fermi-liquid effects, parametrized by the quantity $G^0 \sim 0.16$, is necessary to explain the main features (peaks and dips) of the tunneling spectra, see Figs. 2 and 3. Although these interaction effects are suppressed deep in the superconducting phase, they become more and more important as one moves through the gapless state to the parallel critical-field transition. In the gapless region the effective Fermi-liquid parameter G_{eff}^0 grows quasi-linearly with the quasiparticle density.

Acknowledgments

We gratefully acknowledge enlightening discussions with Ilya Vekhter and Dana Browne. P.W.A. acknowledges the support of the DOE under Grant No. DE-FG02-07ER46420.

-
- * Present address: School of Physics, Georgia Institute of Technology, Atlanta, Georgia 30332, USA
- ¹ L. Landau, Zh. Eksp. Teor. Fiz. **30**, 1058 (1956).
 - ² L. Landau, Zh. Eksp. Teor. Fiz. **32**, 59 (1957).
 - ³ G. Baym and C. Pethick, Landau Fermi-Liquid Theory: Concepts and Applications (John Wiley & Sons, New York, 1991).
 - ⁴ J. A. X. Alexander, T. P. Orlando, D. Rainer, and P. M. Tedrow, Phys. Rev. B **31**, 5811 (1985).
 - ⁵ P. M. Tedrow, J. T. Kucera, D. Rainer, and T. P. Orlando, Phys. Rev. Lett. **52**, 1637 (1984).
 - ⁶ G. A. Gibson, P. M. Tedrow, and R. Meservey, Phys. Rev. B **40**, 137 (1989).
 - ⁷ T. Suzuki, Y. Seguchi, and T. Tsuboi, J. Phys. Soc. Jpn. **69**, 1462 (2000).
 - ⁸ I. L. Aleiner and B. L. Altshuler, Phys. Rev. Lett. **79**, 4242 (1997).
 - ⁹ V. Y. Butko, P. W. Adams, and I. L. Aleiner, Phys. Rev. Lett. **82**, 4284 (1999).
 - ¹⁰ P. W. Adams and V. Y. Butko, Physica B **284-288**, 673 (2000).
 - ¹¹ P. Fulde, Adv. Phys. **22**, 667 (1973).
 - ¹² F. Giazotto, F. Taddei, R. Fazio, F. Beltram, Phys. Rev. Lett. **95**, 066804 (2005); F. Giazotto, F. Taddei, P. D'Amico, R. Fazio, F. Beltram, Phys. Rev. B **76**, 184518 (2007); F. Giazotto, F. Taddei, Phys. Rev. B **77**, 132501 (2008).
 - ¹³ M. Tinkham, "Introduction to Superconductivity", McGraw-Hill, New York (1996).
 - ¹⁴ R. Meservey, P. M. Tedrow, and P. Fulde, Phys. Rev. Lett. **25**, 1270 (1970).
 - ¹⁵ W. Wu and P. W. Adams, Phys. Rev. Lett. **73**, 1412 (1994).
 - ¹⁶ A. M. Clogston, Phys. Rev. Lett. **9**, 266 (1962).
 - ¹⁷ B. S. Chandrasekhar, Appl. Phys. Lett. **1**, 7 (1962).
 - ¹⁸ W. Wu and P. W. Adams, Phys. Rev. Lett. **74**, 610 (1995).
 - ¹⁹ T. Suzuki, T. Tsuboi, and H. Takaki, J. Phys. Soc. Jpn. **53**, 3311 (1984).
 - ²⁰ X. S. Wu, P. W. Adams, G. Catelani, Phys. Rev. Lett. **95**, 167001 (2005); G. Catelani, Phys. Rev. B **73**, 020503(R) (2006).
 - ²¹ K. Maki, in "Superconductivity", edited by R. D. Parks (Dekker, New York, 1969), Chap. 18.
 - ²² V. Y. Butko, P. W. Adams, and E. I. Meletis, Phys. Rev. Lett. **83**, 3725 (1999).
 - ²³ W. Wu, R. G. Goodrich, and P. W. Adams, Phys. Rev. B **51**, 1378 (1995).
 - ²⁴ P. Fulde, Solid State Comm. **5**, 181 (1967).
 - ²⁵ X. S. Wu, P. W. Adams, and G. Catelani, Phys. Rev. B **74**, 144519 (2006).
 - ²⁶ This estimate of ξ is obtained using the value of the mean free path ℓ reported in Ref. 25 via $\xi \simeq \sqrt{\xi_0 \ell}$, where $\xi_0 = \hbar v_F / \pi \Delta_o$ and v_F is the Fermi velocity. To further support this estimate we note that a separate measurement of the perpendicular critical field for similarly prepared a 6-nm-thick film gives $\xi \simeq 56$ nm, (here we use $H_{c\perp} = \phi_0 / 2\pi\xi^2$ with ϕ_0 the flux quantum).
 - ²⁷ see e.g. R. C. Dynes, V. Narayanamurti, J. P. Garno, Phys. Rev. Lett. **41**, 1509 (1978); R. C. Dynes, J. P. Garno, G. B. Hertel, T. P. Orlando, Phys. Rev. Lett. **53**, 2437 (1984).
 - ²⁸ J. P. Pekola, T. T. Heikkilä, A. M. Savin, J. T. Flyktman, F. Giazotto, and F. W. J. Hekking, Phys. Rev. Lett. **92**, 056804 (2004).
 - ²⁹ For example, no broadening is used in the upper panel curve – including it would slightly suppress the peaks' magnitude. Due to their interdependence, however, different values for c and $\Gamma \neq 0$ could also satisfactorily fit the data.